The Astrophysical Journal, 888:71 (10pp), 2020 January 10 https://doi.org/10.3847/1538-4357/ab5d31


# Physical Models for the Clustering of Obscured and Unobscured Quasars

Kelly E. Whalen[1], Ryan C. Hickox[1], Michael A. DiPompeo[1], Gordon T. Richards[2], and Adam D. Myers[3]
[1] Department of Physics & Astronomy, Dartmouth College, 6127 Wilder Laboratory, Hanover, NH 03755, USA
[2] Department of Physics, Drexel University, 3141 Chestnut Street, Philadelphia, PA 19104, USA
[3] Department of Physics and Astronomy, University of Wyoming, Laramie, WY 82071, USA
*Received 2019 July 11; revised 2019 November 22; accepted 2019 November 26; published 2020 January 9*

## Abstract

Clustering measurements of obscured and unobscured quasars show that obscured quasars reside in more massive dark matter halos than their unobscured counterparts. These results are inconsistent with simple unified (torus) scenarios but might be explained by models in which the distribution of obscuring material depends on Eddington ratio or galaxy stellar mass. We test these possibilities by constructing simple physical models to compare to observed active galactic nucleus populations. We find that previously observed relationships between obscuration and Eddington ratio or stellar mass are not sufficient to reproduce the observed quasar clustering results ($\langle \log M_{\rm halo}/M_{\odot} \rangle = 12.94^{+0.10}_{-0.11}$ and $\langle \log M_{\rm halo}/M_{\odot} \rangle = 12.49^{+0.08}_{-0.08}$ for obscured and unobscured populations, respectively) while maintaining the observed fraction of obscured quasars (30%–65%). This work suggests that evolutionary models, in which obscuration evolves on the typical timescale for black hole growth, are necessary to understand the observed clustering of mid-IR-selected quasars.

*Unified Astronomy Thesaurus concepts:* AGN host galaxies (2017); Active galaxies (17); Quasars (1319); Clustering (1908); Galaxy evolution (594)

## 1. Introduction

Quasars, the highly luminous subclass of active galactic nuclei (AGNs), are among the most energetic objects in the universe, and they are powered by supermassive black holes (SMBHs) that are rapidly accreting matter (e.g., Alexander & Hickox 2012). AGNs are often characterized in optical observations by the presence of broad emission features in their spectra, as well as a luminous continuum at rest-frame ultraviolet and optical wavelengths (e.g., Baldwin 1977; Netzer 2015; Padovani et al. 2017). However, there are many observed AGNs that appear to lack one or both of these features. Spectropolarimetric measurements have shown astronomers that these "missing" features are still present, but these photons have been scattered off of some obscuring material before they were observed (e.g., Antonucci & Miller 1985). This leads us to understanding that quasars can be classified as either "obscured" or "unobscured." Here we define a quasar as being obscured if it is shielded by a line-of-sight (LOS) column density ($N_{\rm H}$) of at least $10^{22}\,{\rm cm}^{-2}$ (e.g., Usman et al. 2014; Hickox & Alexander 2018).

The simplest picture of quasar obscuration is that it is an effect due to quasars being randomly oriented relative to an observer. This model of unification by orientation (e.g., Antonucci 1993; Urry & Padovani 1995; Netzer 2015; Ramos Almeida & Ricci 2017) suggests that all AGNs, including quasars, consist of an SMBH with an accretion disk and an axisymmetric distribution of dust, also known as a "dusty torus." The nonspherical geometry of the dusty torus can obscure the nucleus of the AGN for some LOSs, meaning that orientation alone could determine whether or not a quasar is obscured to an observer.

Constraints on this unified picture can be obtained through statistical measurements of the properties of large populations of quasars, both obscured and unobscured. A particularly useful measurable property is spatial clustering, which can determine the masses of the dark matter halos that host quasars and their connection to the large-scale environment, independent of the detailed properties of the individual host galaxies, which can be difficult to measure for luminous AGNs (e.g., Conroy & White 2013; Veale et al. 2014). Until recently, these measurements have focused on optically selected unobscured sources or X-ray-selected AGNs (Croom et al. 2004; Richards et al. 2006; Myers et al. 2007; Ross et al. 2009; Shen et al. 2009; Eftekharzadeh et al. 2015). The dawn of deep, wide mid-IR surveys has allowed us to better understand the environments of obscured quasars (e.g., Werner et al. 2004; Hickox et al. 2007, 2009; Wright et al. 2010; Krumpe et al. 2012; DiPompeo et al. 2014, 2016a, 2017a; Hainline et al. 2014). With a large sample of mid-IR-selected obscured quasars, we can perform statistical analyses to determine whether obscured and unobscured quasars are fundamentally different from one another. For unobscured quasars, spatial clustering measurements have shown that their parent dark matter halo masses are roughly constant across a a redshift range of $0 < z < 5$ (e.g., Croom et al. 2005; Coil et al. 2007; Myers et al. 2007; Shen et al. 2007; da Ângela et al. 2008; Ross et al. 2009; Hickox et al. 2011; Powell et al. 2018). For obscured quasars selected by the *Wide-field Infrared Survey Explorer* (*WISE*; e.g., Wright et al. 2010), it has been measured that for a given redshift, obscured quasars typically reside in higher-mass dark matter halos than their unobscured counterparts (e.g., Hickox et al. 2011; DiPompeo et al. 2014, 2016a, 2017a; Donoso et al. 2014; Powell et al. 2018). For this paper, we will adopt recent measurements from DiPompeo et al. (2017a) that indicate that obscured quasars reside in dark matter halos that have an average mass of $\log M_{\rm halo}/M_{\odot} = 12.94^{+0.10}_{-0.11}$, while unobscured quasars on average reside in dark matter halos of $\log M_{\rm halo}/M_{\odot} = 12.49^{+0.08}_{-0.08}$.[4] These results

[4] We note that DiPompeo et al. (2017a) defined quasar obscuration using an optical/mid-IR color cut of $r - W2 = 6$ (Vega) (e.g., Hickox et al. 2007, 2017) This cut takes advantage of the fact that obscured and unobscured quasars occupy different parts of SDSS/*WISE* color space (e.g., Hickox et al. 2007). Hickox et al. (2017) showed that spectral energy distribution (SED) models are able to predict optical/mid-IR colors for obscured and unobscured quasars that are consistent with observations. The color cut used in DiPompeo et al. (2017a) corresponds to the output of the Hickox et al. (2017) SED model that assumed $A_V = 20$. Based on Equation (3) in Draine (2003), this gives $N_{\rm H} \sim 3.7 \times 10^{22}\,{\rm cm}^{-2}$, which is consistent with our adopted definition of quasar obscuration.

provide observational constraints for any model that tries to explain the relationship between obscured and unobscured quasars.

In contrast with the simplest cases of the unified model of AGNs, quasar obscuration may be a phase in an evolutionary scenario that occurs on timescales of roughly a Salpeter (*e*-folding) time for black hole growth at Eddington-limited accretion. This obscuration phase can be associated with dust structures produced during major galaxy mergers (e.g., Silk & Rees 1998; Springel et al. 2005; Hopkins et al. 2006; Goulding et al. 2012; Treister et al. 2012; Blecha et al. 2018), or it can also be tied to an early phase in a quasar's lifetime at which it is not luminous enough to rid its nucleus of obscuring material (e.g., Hopkins et al. 2008; King 2010). The possibility that obscured and unobscured quasars may represent different evolutionary stages allows for them to have different observed properties such as host galaxy stellar mass, dark matter halo mass, and star formation rate (e.g. Chen et al. 2015; Klindt et al. 2019; Zou et al. 2019).

Many evolutionary models postulate that as dark matter halos grow, black hole growth lags behind (e.g., Alexander et al. 2008; Woo et al. 2008; Kormendy & Ho 2013; DiPompeo et al. 2017b). As these black holes grow in mass, they transition from an obscured phase to an unobscured phase via radiatively driven blowout (e.g., Hopkins et al. 2006, 2008). DiPompeo et al. (2017b) presented a simple evolutionary model in which black hole growth lagged behind galaxy growth. In the DiPompeo et al. (2017b) model, the host dark matter halo grows continuously, while the black hole grows in brief episodes. Here, the black hole's change in mass determines the quasar's evolution from obscuration to being unobscured. Hickox et al. (2007, 2011) showed that bolometric luminosities were similar for populations of obscured and unobscured quasars selected in the mid-IR with the *Spitzer Space Telescope* (Werner et al. 2004). Since luminosity is just a function of Eddington ratio and black hole mass, assuming similar Eddington ratio distributions implies that both unobscured and obscured quasars of a given luminosity should have the same black hole mass, independent of obscuration. In this model, a black hole will begin to grow if it falls too far off the $M_* - M_{\rm BH}$ relation. As the black hole gains mass, the quasar will become luminous enough to rid its nucleus of some obscuring material, and it will then transition from an obscured to an unobscured stage in its evolution. Because the black hole masses of obscured quasars are similar to those of their unobscured counterparts, their dark matter halo masses are predicted to be larger, which is what is empirically seen.

However, it is unclear whether modeling obscuration as an evolutionary stage is the only way to be able to reproduce the difference in average dark matter halo mass ($M_{\rm halo}$) between obscured and unobscured quasars. Although the simplest iterations of the unified model are inconsistent with clustering measurements, the dusty torus clearly plays an important role in quasar obscuration (e.g., Netzer 2015; Ricci et al. 2017; Hickox & Alexander 2018). Ricci et al. (2017) showed that radiative feedback from an AGN could allow for the expulsion of nuclear obscuring dust, thus reducing the number of obscured LOSs between the quasar and observer. Since the amount of radiation pressure exerted on the torus is dependent on the quasar's Eddington ratio ($\lambda_{\rm Edd}$), it is possible that $\lambda_{\rm Edd}$ is driving quasar obscuration. The top panel of Figure 1 shows a schematic of "radiation-regulated unification," in which $\lambda_{\rm Edd}$ determines how much of the quasar is covered by nuclear gas and dust.

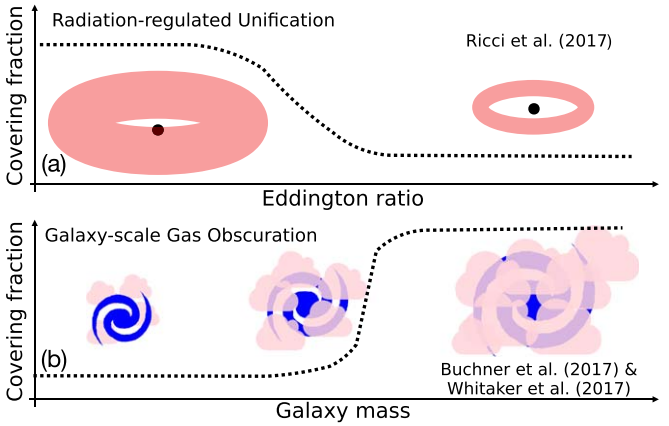


**Figure 1.** (a) Schematic of radiation-regulated unification (Ricci et al. 2017). Studies of X-ray-selected AGNs show that there is a possible relationship between an AGN's covering fraction and its Eddington ratio. Quasars accreting at high fractions of their Eddington luminosities could blow away some of their obscuring, dusty tori via increased radiative pressure, producing a lower fraction of obscured quasars at higher Eddington ratios. (b) Schematic of galaxy-scale gas obscuration (Pannella et al. 2009; Buchner et al. 2017). Empirical relationships between $N_{\rm H}$/covering fraction and galaxy stellar mass have been presented in which less massive galaxies host less obscuring gas than their more massive counterparts. We study these scenarios as possible causes for the mass difference seen in clustering measurements of mid-IR-selected quasars.

It is also possible that quasar obscuration could be taking place in regions outside of the host galaxy's nucleus but is not associated with a specific galaxy's evolutionary stage. Buchner et al. (2017) analyzed the X-ray afterglows of extragalactic long-duration (>2s) gamma-ray bursts (LGRBs) to derive host galaxy gas column densities. From this, they determined a relationship between the stellar mass of a host galaxy and its gas column density in which more massive galaxies have larger average $N_{\rm H}$, and thus more of a probability of obscuring a central quasar. Pannella et al. (2009) and Whitaker et al. (2017) found a similar dependence of the fraction of obscured star formation on host galaxy stellar mass. Since star formation in massive galaxies is being obscured by interstellar gas and dust, it may be expected that a central quasar would also be obscured. A schematic of galaxy-scale obscuration is shown in the bottom panel of Figure 1.

In this work, we test these simple models of radiation-regulated unification and galaxy-scale obscuration to determine whether they can generate populations of simulated quasars that are consistent with observations of mid-IR-selected quasars. We also probe the effect that a luminosity cut that is representative of the limits of *WISE* has on the $M_{\rm halo}$ of our simulated obscured and unobscured quasar populations.

Definitions to frequently used terms are given in Table 1. We adopt a cosmology of $H_0 = 70.2\,{\rm km\,s^{-1}\,Mpc^{-1}}$, $\Omega_M = \Omega_{\rm CDM} + \Omega_b = 0.229 + 0.046 = 0.275$, and $\Omega_\Lambda = 0.725$ (Komatsu et al. 2011).

## 2. The Models

In this section we describe how we construct our simple models of quasar obscuration based on known halo mass and $\lambda_{\rm Edd}$ distributions, as well as empirical relationships between obscuring fraction and $\lambda_{\rm Edd}$ and between obscuring fraction and host galaxy stellar mass.

**Table 1**
Definitions of Terms Used throughout This Work

| Term | Definition |
|---|---|
| Obscured quasar | Quasar that is shielded by LOS $N_H \gtrsim 10^{22}$ cm$^{-2}$ (e.g., Usman et al. 2014; Hickox & Alexander 2018) |
| Covering fraction ($f_{cov}$) | Probability of an observer having an obscured LOS to a quasar based on the physical distribution of obscuring material (e.g., Ricci et al. 2017) |
| Obscured fraction ($f_{obsc}$) | Fraction of quasars in a given population that are obscured |

### 2.1. Generating the Quasar Sample

We begin by generating a model population of 10 million dark matter halos randomly and uniformly distributed in logarithmic space in the mass range $10^{10} M_\odot < M_{halo} < 10^{16} M_\odot$. Each of these sample halos was assigned a weight using the $z = 1$ halo mass function (HMF) detailed in Tinker et al. (2010) so that each halo's contribution to the total average is proportional to the space density of halos of that mass. We used a CAMB (Lewis et al. 2000) generated matter power spectrum to compute the HMF. Weighting our uniformly and randomly distributed sample of host halos by the HMF eliminates shot noise in our simulated data. This is because even though our rare, high-mass halos will have a small contribution to the average host halo mass, they are still equally as numerous in our simulation as their low-mass counterparts.

Once we produced a weighted sample of halos across a wide mass range, we calculated the stellar masses of their corresponding galaxies using the $z = 1$ halo mass–stellar mass relationship presented in Moster et al. (2010). The distribution of our simulation galaxies in stellar mass space is consistent with observed $z \sim 1$ stellar mass functions (e.g., Pérez-González et al. 2008; Behroozi et al. 2010). We then calculated the masses of the central black holes of each galaxy with the stellar mass–black hole mass relationship detailed in Häring & Rix (2004). Again, we find that the black hole mass distribution of our simulated quasars is broadly consistent with observed black hole mass functions (e.g., Shankar et al. 2009; Kelly & Merloni 2012). There is intrinsic scatter in both the halo mass–stellar mass and stellar mass–black hole mass relationships, so we included these effects in our models. We adopted an intrinsic scatter of 0.2 dex for the halo mass–stellar mass relationshiop and 0.3 dex for the stellar mass–black hole mass relationship (Häring & Rix 2004; Moster et al. 2010).

We generated a separate sample of 10 million Eddington ratios that are randomly and uniformly distributed in logarithmic space in the range $-4 < \log \lambda_{Edd} < 1$. Just as we assigned weights to each dark matter halo based on the HMF, we also assigned weights to each $\lambda_{Edd}$ that correspond to the double power-law–$\lambda_{Edd}$ distribution presented in Jones et al. (2019) to limit the contribution of rare, high-Eddington systems to the overall distribution. The overall probability of a halo of a given mass containing a quasar accreting at a particular $\lambda_{Edd}$ is the product of the HMF and the $\lambda_{Edd}$ distribution function.

Although we can use this treatment to generate quasars of all luminosities, observational surveys are limited by their capabilities to detect faint sources. Our model therefore needs to include a lower luminosity limit so we can match our quasar distributions to observations. We first calculate the bolometric luminosities for all of our generated quasars. Since we are interested in mid-IR-selected quasars, we implement a luminosity threshold that is representative of the detection limits of *WISE*. Bolometric luminosities for *WISE*-selected quasars at $z = 1$ are typically greater than $10^{46}$ erg s$^{-1}$ (e.g., Hickox et al. 2007; Assef et al. 2013), so we impose a luminosity limit of $10^{45.8}$ erg s$^{-1}$ following DiPompeo et al. (2017b) unless otherwise stated.

### 2.2. Identifying Obscured Sources

Creating obscured and unobscured populations of quasars from the simulated sample requires us to adopt a model that parameterizes obscuration as a function of one of the physical properties of either the quasars or their host galaxies. Broadband observations of quasars can tell us whether or not a given source is obscured (e.g., Merloni et al. 2014), but they do not necessarily yield information with respect to the scale at which the light emitted from the quasar is being absorbed. We first assume that our quasars are being obscured by their dusty tori, and we adopt the radiation-regulated unification model in which obscuration is parameterized by the $\lambda_{Edd}$ of our quasars (Ricci et al. 2017). For galaxy-scale interstellar material, we parameterize obscuration as a function of host galaxy stellar mass (Pannella et al. 2009; Buchner et al. 2017; Whitaker et al. 2017). We also present a model that allows our simulated quasars to be obscured by both their tori and the interstellar material in their host galaxies. In what follows, we describe the details of each model.

#### 2.2.1. Radiation-regulated Unification Model

Ricci et al. (2017) presented the relationship between the covering fractions of AGNs and their $\lambda_{Edd}$. This relationship was derived from a multiwavelength study of 836 AGNs identified by the *Swift*/BAT X-ray survey (e.g., Gehrels et al. 2004; Barthelmy et al. 2005; Baumgartner et al. 2013; Krimm et al. 2013). We used the observed relationship shown in Figure 4 of Ricci et al. (2017) to model a population of obscured and unobscured AGNs where the obscured fraction depends on $\lambda_{Edd}$. We chose to use this relationship over the one detailed in Figure 1 of Ricci et al. (2017) to account for the existence of Compton-thick material that might obscure the most highly accreting quasars. Although this was originally presented for AGNs at $z \sim 0.1$, we expect it to hold for our model at $z = 1$. Observations of high-redshift quasars have shown that there is not much evolution over cosmic time on the $\lesssim$1 pc scale at which radiation-regulated feedback would be significant (e.g., Fan 2006; Lusso & Risaliti 2016).

The data bins used in Ricci et al. (2017) to average covering fractions at a given $\lambda_{Edd}$ were broad, so we made this relationship more continuous over a range of $\lambda_{Edd}$ by fitting a series of error functions to the original data, as seen in Figure 2. Each fit corresponds to varying the minimum $f_{cov}$ for high-accreting quasars (the covering fractions in the Compton-thick regime are not well constrained). The gray shaded region in Figure 2 represents the errors on the $f_{cov} - \log \lambda_{Edd}$ relationship shown in Figure 4 of Ricci et al. (2017). Using these $f_{cov} - \log \lambda_{Edd}$ relationships, we then randomly assigned the quasars to obscured and unobscured populations. We do this by

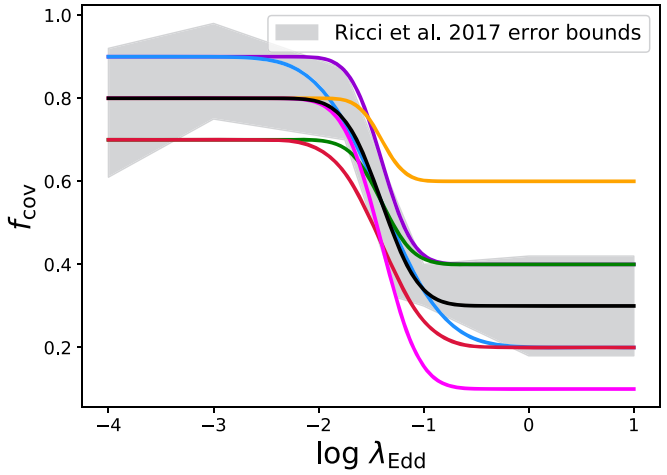


**Figure 2.** Relationship between covering fraction and $\lambda_{Edd}$ for the radiation-regulated unification model presented in Ricci et al. (2017). The error bounds from Figure 4(a) in Ricci et al. (2017) are shown in gray. We modeled this relationship as error functions that spanned the parameter space occupied by the error bounds in Ricci et al. (2017). We also included two model fits that fall outside of the Ricci et al. (2017) error bounds to account for the uncertainty on the Compton-thick fraction.

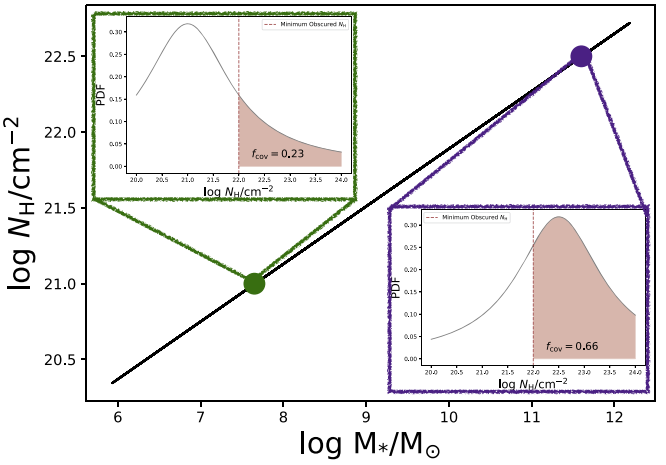


**Figure 3.** Schematic of how covering fractions are calculated from assigned $N_H$ values. Each galaxy is assigned a mean $N_H$ based on its $M_*$. Each galaxy's mean $N_H$ is then used as the mean of a column density pdf that is then integrated on the interval $10^{22} < N_H/\mathrm{cm}^{-2} < \infty$ to determine the covering fraction at each given $M_*$.

assigning each quasar a random number between zero and one. If this number is less than or equal to $f_{cov}$ at a quasar's $\lambda_{Edd}$, then it is classified as obscured. Otherwise, it is classified as unobscured.

We also note that for some populations of quasars at higher redshifts it is possible for the accretion disk to have a "slim-disk" geometry in which the accretion disk is puffed up for the quasars that are accreting at high $\lambda_{Edd}$ (e.g., Frank et al. 2002; Leighly 2004; Luo et al. 2015). The thin disk is geometrically thin and optically thick, so in principle this could contribute to obscuration in addition to the dusty torus. As for the $f_{cov}$–$\lambda_{Edd}$ relationships in Figure 2, this effect would increase $f_{cov}$ again at high $\lambda_{Edd}$. We consider the effect of slim accretion disk geometries below, but this scenario is more applicable for luminous quasars at $z \sim 2$ than the population we are simulating (e.g., Netzer & Trakhtenbrot 2014).

### 2.2.2. Galaxy-scale Obscuration

The radiation-regulated unification model assumes that the quasars are being obscured by the parsec-scale dusty torus and that the $\lambda_{Edd}$ of the quasar could change the covering fraction of the torus. However, toroidal dust is not the only obscuring material in front of the quasar along the LOS of an observer. Interstellar gas and dust within a galaxy could have the ability to obscure a quasar at the galactic center (e.g., Hickox & Alexander 2018).

Buchner et al. (2017) measured the attenuation of X-ray afterglows from extragalactic LGRBs to derive an empirical relationship between the mean column densities of gas in galaxies and their stellar masses. This relationship shows that more massive galaxies contain deeper obscuring columns of gas. Knowing the $N_H$ of gas in galaxies can allow us to determine the likelihood of obscuration for a given quasar. Buchner & Bauer (2017) used the log $N_H$–log $M_*$ relationship derived in Buchner et al. (2017) to construct a simple model of obscuring covering fractions for AGNs. Here, we study this model to determine whether it is capable of re-creating clustering measurements of mid-IR-selected quasars.

We start by using the GRB-derived log $N_H$–log $M_*$ relationship from Buchner et al. (2017) to assign each of our simulated galaxies a mean $N_H$. We assume that the assigned $N_H$ is the mean of a column density probability distribution. Here, we use a Gaussian probability density function (pdf) with $\sigma = 0.5$, as well as a Student's $t$-distribution with 1 degree of freedom. The Student's $t$-distribution acts as a proxy for the broader, less peaked SingleEllipse model detailed in Buchner et al. (2017) since the two models have a similar analytic form (J. Buchner 2019, private communication). X-ray-selected AGNs are typically detected as obscured when $N_H > 10^{22}\mathrm{cm}^{-2}$ (e.g., Predehl & Schmitt 1995; Burtscher et al. 2016; Schnorr-Müller et al. 2016), and this generally corresponds to the $N_H$ of mid-IR-selected quasars (e.g., Hickox et al. 2007; Usman et al. 2014). We convert the mean column densities from the log $N_H$–log $M_*$ relationships to effective covering fractions by integrating each of the $N_H$ pdf's on the interval $10^{22} < N_H/\mathrm{cm}^{-2} < \infty$, as depicted in Figure 3. The covering fraction–stellar mass relationships derived using the Gaussian and Student's $t$-distributions are shown as the blue and red curves in Figure 4, respectively.

In addition to the GRB X-ray afterglow attenuation-derived models described above, we also calculated an $f_{cov}$–log $M_*$ relationship based on the galaxy mass dependence of the fraction of obscured star formation in galaxies presented in Whitaker et al. (2017). The simple assumption here is that the material obscuring star formation in these galaxies will similarly obscure quasar activity. Pannella et al. (2009) presented a relationship between UV attenuation and stellar mass. We utilized this relationship to derive LOS column densities as a function of stellar mass since it is unclear how the fraction of obscured star formation in a galaxy relates to the physical dust distribution. Whitaker et al. (2017) showed that the obscured star formation fractions derived from the Pannella et al. (2009) relationship were consistent with what they calculated from IR and UV star formation rates.

We convert the Pannella et al. (2009) UV attenuation–stellar mass relationship to a column density–stellar mass relationship by assuming an $R(V) = 3.1$ (Milky Way) extinction curve (e.g., Fitzpatrick 1999; Draine 2003). At 1500 Å, this corresponds to $A_{1500}/N_H = 1.6 \times 10^{-21}\frac{\mathrm{cm}^2\mathrm{mag}}{\mathrm{H}}$. We note that the UV

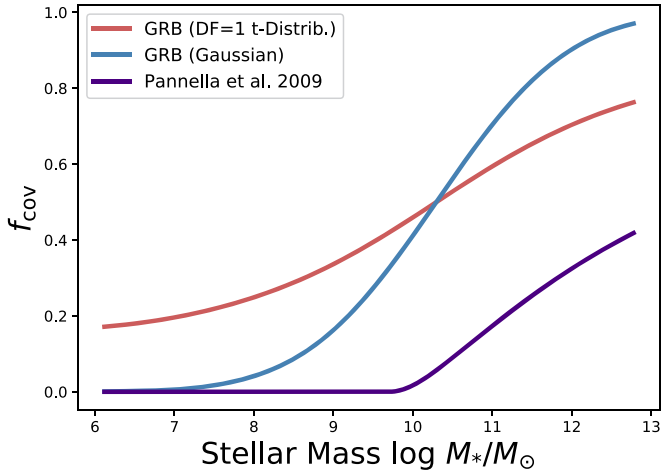


**Figure 4.** Relationships between covering fraction and host galaxy stellar mass. Using the mean $N_H$ at a given stellar mass, we calculated covering fractions as detailed in Section 2.2.2. These relationships are used to produce model populations of obscured and unobscured quasars based on obscuration by galaxy-scale gas.

attenuation–stellar mass relationship in Pannella et al. (2009) is fitted over a much smaller stellar mass range than included in our simulated sample. However, once we enact a luminosity threshold, only ∼12% of our sources fall outside the Pannella et al. (2009) stellar mass range, and of those sources, ∼88% fall within 0.3 dex of the fitted mass range, so we are confident in the extrapolation of this relationship. We then compute an $f_{cov}$–$M_*$ relationship using the same methodology as done with the models derived from the attenuation of GRB X-ray afterglows.

## 3. Results

Our models need to be able to recover the following observational constraints: (1) the host $M_{halo}$ for our simulated obscured and unobscured quasars, as well as (2) the fraction of obscured quasars. The measured average host $M_{halo}$ of obscured and unobscured quasars are $\log M_{halo}/M_\odot = 12.94^{+0.10}_{-0.11}$ and $\log M_{halo}/M_\odot = 12.49^{+0.08}_{-0.08}$, respectively (e.g., DiPompeo et al. 2017a). The range of observed obscured fractions for luminous quasars is roughly between 30% (Treister et al. 2008) and 65% (Polletta et al. 2008), with significant uncertainty on the heavily obscured (Compton-thick) population (e.g., DiPompeo et al. 2016b; Yan et al. 2019). We note that we adopt such a broad observed obscured fraction to reflect the uncertainty due to the difficulty of detecting heavily obscured AGNs. This is a conservative estimate that provides a broad parameter space in which our models could be potentially viable.

### 3.1. Radiation-regulated Unification Model

As seen above in Figure 2, we modeled radiation-regulated unification as a series of error functions within the $f_{cov}$–$\lambda_{Edd}$ parameter space covered by the error bounds of the relationship shown in Figure 4(a) of Ricci et al. (2017). We also included two parameterizations that were well above and below the error bounds to account for the uncertainty in the Compton-thick fraction of quasars. We calculated $f_{obsc}$ for each of these models and found that $f_{obsc}$ is roughly equal to the value of $f_{cov}$ at high $\lambda_{Edd}$. This is because the luminosity cut pushes the mean of the underlying Eddington ratio distribution to be $\log\langle\lambda_{Edd}\rangle \approx 0$. Since there is little dynamic range in $f_{cov}$ at high $\lambda_{Edd}$, $f_{obsc}$ becomes the assigned high-$\lambda_{Edd}$ $f_{cov}$ value. The implication of this for our simulated populations is that only the three parameterizations with high-$\lambda_{Edd}$ $f_{cov} \geqslant 0.3$ satisfy $f_{obsc}$ constraints. In what follows, we focus on the model fit (shown in black in Figure 2) that is the mean of the Ricci et al. (2017) error bounds. We use this relationship since it produced a population of quasars whose $f_{obsc}$ falls on the edge of the observed obscured fraction range, as well as because it best represents the results presented in Ricci et al. (2017).

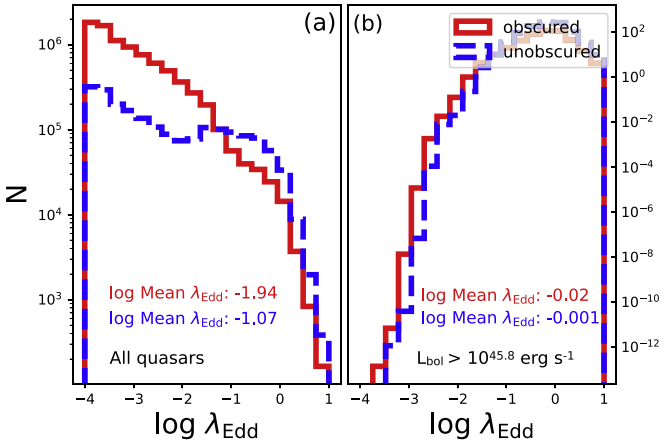


**Figure 5.** (a) Full weighted distributions of $\lambda_{Edd}$ for our simulated quasars generated using the mean of the Ricci et al. (2017) error bounds on $f_{cov} - \log\lambda_{Edd}$ (black curve in Figure 2). Obscured quasars are shown in red bins, and unobscured quasars in blue. There is an intrinsic difference in the $\lambda_{Edd}$ distributions between the obscured and unobscured populations of quasars owing to the fact that the chosen $f_{cov} - \log\lambda_{Edd}$ relationship preferentially obscures low-$\lambda_{Edd}$ quasars. (b) Distribution of $\lambda_{Edd}$ after a luminosity cut of $10^{45.8}$ erg s$^{-1}$, corresponding to *WISE*-selected quasars (e.g., DiPompeo et al. 2017b). The luminosity cut causes our model to exclude the low-$\lambda_{Edd}$ end of our initial distributions, thus pushing our populations to become increasingly similar.

For this $f_{cov} - \log\lambda_{Edd}$ relationship, we examined the $\lambda_{Edd}$ and host $M_{halo}$ distributions for the generated obscured and unobscured populations of quasars. Figure 5 presents the full $\lambda_{Edd}$ distribution for our simulated quasars, as well as the distribution after a luminosity cut of $10^{45.8}$ erg s$^{-1}$ has been applied (e.g., DiPompeo et al. 2017b). Initially, there is an intrinsic difference between the shapes of the obscured and unobscured $\lambda_{Edd}$ distributions. As expected, the unobscured population has a higher mean $\lambda_{Edd}$ than its obscured counterpart owing to the fact that the shape of the $f_{cov} - \log\lambda_{Edd}$ distribution dictates that low-$\lambda_{Edd}$ quasars have a higher probability of being obscured. However, applying a lower luminosity limit causes us to lose the low-$\lambda_{Edd}$ end where the two populations are the most distinct from one another. This effectively makes the mean $\lambda_{Edd}$ identical for the populations of obscured and unobscured quasars.

Figure 6 shows the corresponding host $M_{halo}$ distributions. In this model, obscuration is independent of host $M_{halo}$, so our distributions for the full populations of simulated obscured and unobscured quasars are identical. The initial $f_{obsc}$ for the full sample is 78%, dropping to 29% for the luminosity cut, thus removing a significant number of our obscured quasars that reside in low-mass dark matter halos. The removal of obscured quasars in low-mass halos results in a small difference between the average host $M_{halo}$ for the obscured and unobscured populations, but it is still well outside of our observational constraints.

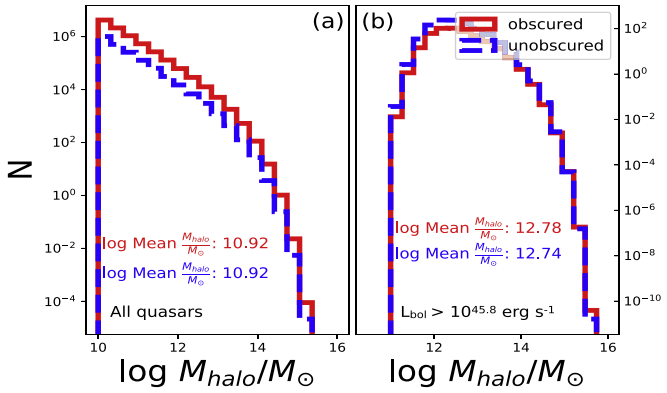


**Figure 6.** (a) Full weighted distributions of host $M_{\rm halo}$ for our simulated quasars generated using the mean of the Ricci et al. (2017) error bounds on $f_{\rm cov}-\log\lambda_{\rm Edd}$ (black curve in Figure 2). Obscured quasars are shown in red bins, and unobscured quasars in blue. (b) Distributions of host $M_{\rm halo}$ for our sample quasars after a luminosity cut of $10^{45.8}$ erg s$^{-1}$, corresponding to *WISE*-selected quasars (e.g., DiPompeo et al. 2017b). The obscured and unobscured populations have the same mean $M_{\rm halo}$ before the luminosity cut and only a negligible post-cut difference that falls outside of our observational constraint on mean $M_{\rm halo}$.

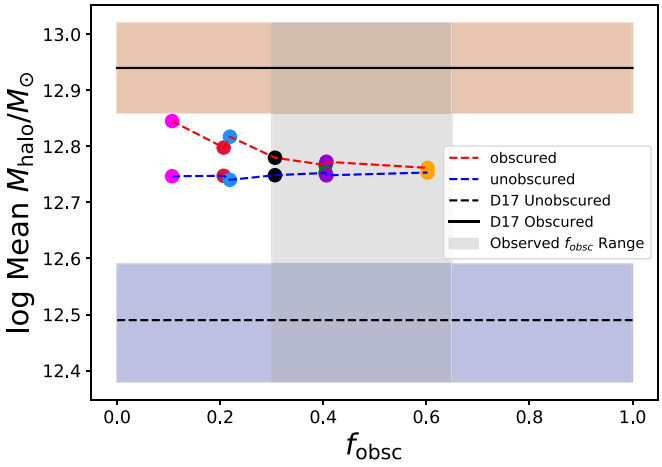


**Figure 7.** Calculated mean halo masses for simulated quasar populations generated using different error function fits to the $f_{\rm cov}-\log\lambda_{\rm Edd}$ relationship as seen in Figure 2. The solid black line shows the mean halo mass of a population of observed obscured quasars (e.g., DiPompeo et al. 2017a), where the red shaded region shows the error on that measurement. This is also the case for the black dashed line and the blue shaded region, but for the unobscured population studied in DiPompeo et al. (2017a). Each point corresponds to the populations generated using the model of the same color in Figure 2. The points connected by the red (blue) dashed line are the average obscured (unobscured) host halo masses. The radiation-regulated unification model is unable to recover both the disparity in $M_{\rm halo}$ between obscured and unobscured quasars and an obscured fraction that falls within the range of observations.

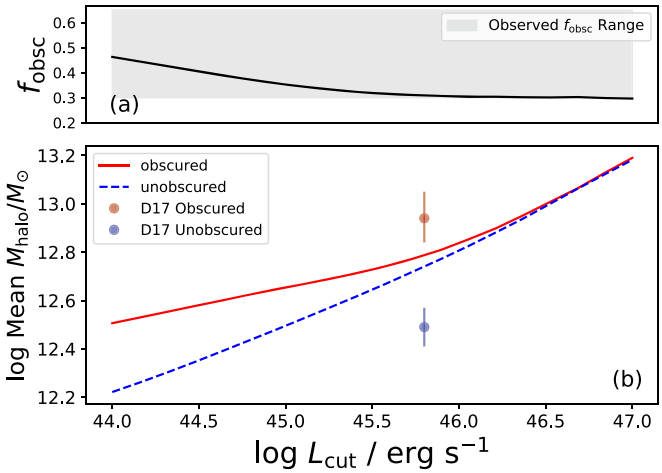


**Figure 8.** (a) Obscured fraction of our sample population modeled from the yellow curve in Figure 2 as a function of the luminosity threshold for the radiation-regulated unification model. At every luminosity limit, the obscured fraction resides within the range of observed obscured fractions. (b) Relationship between the weighted mean $M_{\rm halo}$ of the distribution and the luminosity threshold. The obscured sample is depicted by the solid red line, and the unobscured sample is depicted by the dashed blue line. It is apparent that the choice in luminosity limit affects the disparity between the mean $M_{\rm halo}$ for obscured and unobscured quasars, but it does not reproduce observations.

We next carry out this analysis for all of the parameterizations of our radiation-regulated unification model, as seen in Figure 2. Just as we calculated the fraction of obscured quasars for each $f_{\rm cov}-\log\lambda_{\rm Edd}$ relationship, we also calculated mean host $M_{\rm halo}$ for the generated populations of obscured and unobscured quasars. These are presented in Figure 7. The red and blue shaded regions show the uncertainty for the measured mean $M_{\rm halo}$ for mid-IR-selected obscured and unobscured quasars, respectively (DiPompeo et al. 2017a). We find that as we increase the covering fraction at high $\lambda_{\rm Edd}$, the mean $M_{\rm halo}$ for obscured and unobscured quasars become increasingly similar. Increasing the covering factor for high-$\lambda_{\rm Edd}$ sources at a given luminosity threshold allows for more low-mass, high-$\lambda_{\rm Edd}$ quasars to be classified as obscured. For a luminosity cut of $10^{45.8}$ erg s$^{-1}$, there is nowhere in this parameter space that satisfies both the mass difference and obscured fraction observational constraints.

Following DiPompeo et al. (2017b), we probed the effect the luminosity cut had on our simulated quasar populations. For the population of quasars generated from the minimum $f_{\rm cov}=0.3$ model, we find that as the luminosity cut increases, the mean $M_{\rm halo}$ for the obscured and unobscured populations converge. Increasing the minimum detectable luminosity effectively pushes our sample to be composed of quasars that are either accreting at higher $\lambda_{\rm Edd}$ or residing in higher-mass dark matter halos. As also shown in Figures 5 and 6, increasing the lower luminosity limit excludes the low-Eddington end of our quasar populations, where their $\lambda_{\rm Edd}$ distributions are most distinct from one another. Our model is able to produce a $\sim$0.3 dex difference in $M_{\rm halo}$ for obscured and unobscured quasars at low-luminosity cuts (around $10^{44}$ erg s$^{-1}$), which is still even smaller than the observed difference shown in DiPompeo et al. (2017a). This is shown in Figure 8. Overall, the difference between simulated $M_{\rm halo}$ for our obscured and unobscured populations falls significantly below observations.

As mentioned earlier at the end of Section 2.2.1, we also considered the effect of obscuration due to a slim accretion disk at high $\lambda_{\rm Edd}$. We did this by implementing a linear increase of $f_{\rm cov}$ starting at $\log\lambda_{\rm Edd}=0$ such that a quasar with $\log\lambda_{\rm Edd}=1$ has a covering fraction of 1. We found that implementing a slim accretion disk in the model with minimum $f_{\rm cov}=0.3$ mildly decreased the average $M_{\rm halo}$ for our obscured population of quasars, making it identical to the average unobscured quasar dark matter halo mass. The average $M_{\rm halo}$ for the simulated obscured and unobscured quasars are both $\log M_{\rm halo}/M_\odot=12.75$. This, in addition to the fact that slim accretion disks are

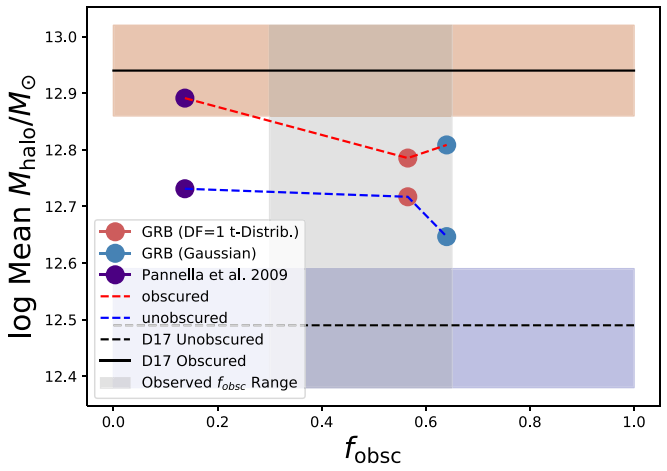


**Figure 9.** Calculated mean $M_{\rm halo}$ for simulated quasar populations generated using $f_{\rm cov}-\log M_*$ relationships as seen in Figure 4. The red (blue) dashed line connects the average host halo mass for the obscured (unobscured) population generated from the $f_{\rm cov}-\log M_*$ of the same color from Figure 4. The solid black line shows the measured mean $M_{\rm halo}$ of a population of observed obscured quasars (e.g., DiPompeo et al. 2017a), where the red shaded regions show the errors on that measurement. This is also the case for the black dashed line and the blue shaded region, but for the unobscured population studied in DiPompeo et al. (2017a). Although these models are able to drive small differences in average $M_{\rm halo}$ for obscured and unobscured quasars, they do not satisfy observational constraints.

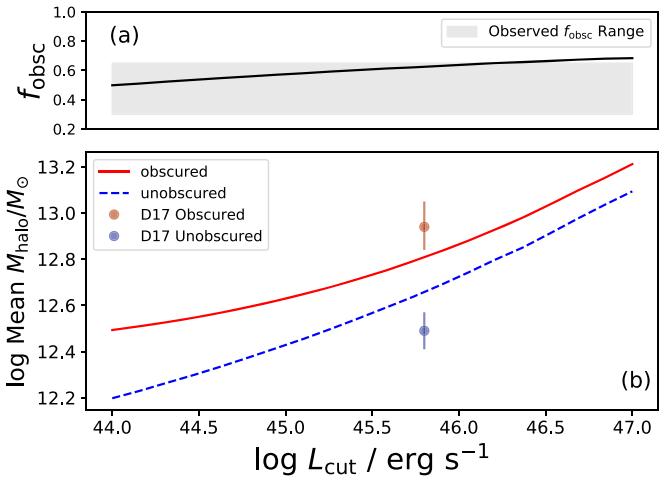


**Figure 10.** (a) Obscured fraction for the populations of quasars generated at each varying luminosity threshold for the observed GRB-derived Gaussian galaxy-scale dust model of obscuration (as shown in blue in Figure 4 and thereafter). (b) Relationship between the mean $M_{\rm halo}$ of our obscured (red solid curve) and unobscured (blue dashed curve) populations and luminosity threshold. For this obscuration model, the choice in luminosity limit minimally affects the disparity between the mean $M_{\rm halo}$ for obscured and unobscured quasars, but it does not reproduce observations.

also more often found in luminous, $z\sim 2$ AGNs rather than in the $z\sim 1$ quasar populations we are modeling (e.g., Netzer & Trakhtenbrot 2014), shows us that this model is not viable for re-creating mid-IR quasar clustering measurements.

### 3.2. Galaxy-scale Gas Obscuration

Here we conduct a similar analysis to that for the radiation-regulated unification model, instead assuming that the obscurer is galaxy-scale gas, to determine whether this model could satisfy observational constraints.

As before, we calculated obscured fractions and mean $M_{\rm halo}$ values for the populations of quasars that were generated using the various $f_{\rm cov}-\log M_*$ relationships shown in Figure 4. The calculated obscured fraction for each $f_{\rm cov}-\log M_*$ relationship is shown as the $x$-axis of Figure 9. It is apparent that two of the $f_{\rm cov}-\log M_*$ relationships produced populations of quasars that were more highly obscured than what has been observed since the points for these models fall outside of the gray box that depicts the range of observed obscured fractions. For a quasar to be luminous enough to be detectable using mid-IR color selection, it would have to be rapidly accreting or host a massive black hole. Since we are considering the galaxy stellar-mass-dependent model here, as well as scaling relationships between $M_{\rm BH}$ and $M_*$, the quasars that would be detectable in this model will typically reside in galaxies with large stellar masses. Since the $f_{\rm cov}-\log M_*$ relationships in Figure 4 state that more massive galaxies have a higher probability of obscuring the central quasar, this results in the populations of quasars generated with the Gaussian Buchner et al. (2017) inspired model having a higher obscured fraction than observed. The mean $M_{\rm halo}$ values are shown as the $y$-axis in Figure 9. Much like what occurred in the results of the radiation-regulated unification model, we find that the weighted mean parent $M_{\rm halo}$ for all of the $f_{\rm cov}-\log M_*$ relationships fall outside of the range of clustering measurements, which is shown by the red (blue) shaded region for observed obscured (unobscured) sources.

Figure 10 shows our GRB-derived Gaussian galaxy-scale gas obscuration model's dependence on luminosity cut. We chose this model because it produced an $f_{\rm obsc}$ that fell on the edge of observational constraints, as well as having a modest difference between $M_{\rm halo}$ of its obscured and unobscured quasar populations. The intrinsic $M_{\rm halo}$ distributions created by the galaxy-scale gas models are most different from one another at low $M_{\rm halo}$. Once again, a higher-luminosity cut results in sampling a region in the original $M_{\rm halo}$ distribution where the obscured and unobscured distributions are almost indistinguishable. It is clear that modeling a quasar's obscuration as a function of its host galaxy's stellar mass is not sufficient to properly recover clustering measurements of parent $M_{\rm halo}$, as well as the observed quasar obscured fraction.

### 3.3. Combining Nuclear and Galaxy-scale Obscuration

Both of the models discussed above assume that obscuration is coming from material either within the region closest to the quasar or within the interstellar regions of the host galaxy. We next consider that there could be many possible LOSs in which the obscuring material is independently contributed by both the nuclear-scale torus and the galaxy-scale gas and dust. Here we adopt a $\log N_{\rm H}-\log\lambda_{\rm Edd}$ relationship from Ricci et al. (2017) to assign our quasars nuclear column densities. We then sum the nuclear and the Buchner et al. (2017) assigned galaxy-scale column densities to obtain a mean LOS column density for each of the sources in our simulated sample. Utilizing the same methodology described above in Section 2.2.2, these mean LOS column densities are treated as the mean of a Gaussian pdf that is integrated on the interval $10^{22}<N_{\rm H}/{\rm cm}^{-2}<\infty$ to obtain an LOS covering fraction for each quasar. We again randomly assign our quasars into obscured and unobscured populations based on their calculated covering fractions. We find that after applying the luminosity cut, the mean $M_{\rm halo}$ for the obscured and unobscured populations are $\log M_{\rm halo}/M_\odot=12.79$ and $\log M_{\rm halo}/M_\odot=12.65$, respectively, and that $f_{\rm obsc}=0.75$. This

**Table 2**
Effect of Shifting Black Hole Masses of Our Modeled Quasars

| Model | $\log M_{\rm BH}/M_{\odot}$ Shift (dex) | Obscured Mean ($\log M_{\rm halo}/M_{\odot}$) | Unobscured Mean ($\log M_{\rm halo}/M_{\odot}$) | $f_{\rm obsc}$ |
|---|---|---|---|---|
| Radiation-regulated | −0.5 | 12.94 | 12.92 | 0.27 |
| | 0.0 | 12.80 | 12.75 | 0.28 |
| | +0.5 | 12.70 | 12.59 | 0.30 |
| Galaxy-scale (Pannella) | −0.5 | 13.03 | 12.90 | 0.16 |
| | 0.0 | 12.91 | 12.75 | 0.14 |
| | +0.5 | 12.80 | 12.59 | 0.12 |
| Galaxy-scale (GRB Gaussian) | −0.5 | 12.97 | 12.83 | 0.67 |
| | 0.0 | 12.82 | 12.65 | 0.63 |
| | +0.5 | 12.65 | 12.57 | 0.61 |
| Galaxy-scale (GRB *t*-dist.) | −0.5 | 12.96 | 12.90 | 0.58 |
| | 0.0 | 12.79 | 12.72 | 0.56 |
| | +0.5 | 12.77 | 12.71 | 0.57 |
| Nuclear + galaxy | −0.5 | 12.94 | 12.83 | 0.77 |
| | 0.0 | 12.79 | 12.65 | 0.75 |
| | +0.5 | 12.66 | 12.48 | 0.73 |

model overpredicts the number of obscured quasars in this population, and it is unable to reproduce the magnitude of the mass discrepancy between the host halos of obscured and unobscured quasars. It is possible that torus and galaxy-scale obscuration (as modeled here) can contribute to this observed host mass difference to some degree but cannot reproduce the observational results. This suggests that evolutionary models in which obscuration is an earlier stage in the lifetime of the quasar may be necessary to recover observed properties of mid-IR-selected quasars.

### 3.4. The Effects of Uncertainty

Here we address the various sources of uncertainty in our models, as well as their effects on our results.

#### 3.4.1. Uncertainty in Scaling Relationships

There is a degree of uncertainty inherent in the relationships that allowed us to convert our simulated $M_{\rm halo}$ into galaxy stellar masses and then into black hole masses (e.g., Häring & Rix 2004; Moster et al. 2010). These uncertainties get propagated through each conversion, and they are exacerbated by the fact that these uncertainties are higher for the relationships at $z = 1$ than in the local universe (e.g., Häring & Rix 2004; Behroozi et al. 2010; Guo et al. 2010; Lamastra et al. 2010; Moster et al. 2010). There is also uncertainty in the observed stellar mass and black hole mass functions out at higher redshifts (Kelly & Merloni 2012; Kormendy & Ho 2013). To account for possible effects of uncertainty in the black hole masses at $z = 1$, we probed the effect of shifting our black hole masses by ±0.5 dex for our radiation-regulated unification and galaxy-scale gas obscuration models, in accordance with the maximum error propagated through scaling relationships, as estimated in Kelly & Merloni (2012). This shift in black hole mass for our simulated quasars effectively changes the number of quasars that can be detectable after a luminosity cut is enacted, thus changing the shape of the mass distributions of our obscured and unobscured quasars.

The results for this analysis are presented in Table 2. Shifting the black hole masses of our sample by ±0.5 dex did not have a strong impact on the obscured fractions for any of our models. However, since shifting our black hole masses effectively changed our luminosity cut, there was a noticeable difference in the calculated obscured and unobscured mean $M_{\rm halo}$. On average, shifting our black hole masses by −0.5 dex pushed all of the obscured and unobscured quasars to reside in more massive halos since we essentially excluded any quasars that were initially on the cusp of the luminosity cutoff. For all of the models, the shift in black hole mass of −0.5 dex produced populations of quasars whose host dark matter halos are more massive than observed, as well as obscured and unobscured populations that reside in dark matter halos of similar masses. When we shifted our black hole masses by +0.5 dex, we allowed more of our quasars to survive the luminosity cut applied. This shift had the effect of lowering the mean $M_{\rm halo}$ for all of the obscured and unobscured populations of quasars that our models generated. Even though the mass difference between each of the obscured and unobscured populations is greater than that of the original, unshifted populations, all of the mean dark matter halos for the obscured quasars fall below that of clustering measurements.

Overall, we find that even with this systematic shift in black hole masses, our models are unable to satisfy all of the observational constraints.

#### 3.4.2. Uncertainty in Covering Fraction Parameterizations

As shown above in Figure 2, there are formal uncertainties on the $f_{\rm cov} - \log \lambda_{\rm Edd}$ relationship presented in Ricci et al. (2017). In our primary analysis, we mostly considered the effect of the highly uncertain Compton-thick fraction on our models. This is because the *WISE* luminosity limit eliminates the low-$\lambda_{\rm Edd}$ quasars from our sample (as seen in Figure 5), so only differences in $f_{\rm cov}$ at high $\lambda_{\rm Edd}$ should affect our simulated sample. However, for completeness we also explored the entire parameter space occupied by the error bounds on the original Ricci et al. (2017) relationship. We tested models that had low-$\lambda_{\rm Edd}$ covering fractions toward the high end and the low end of the formal error bounds, as well as the same at the high-$\lambda_{\rm Edd}$ end of the relationship. We found that none of our models that spanned the range of the Ricci et al. (2017) error bounds were able to drive significant differences between the mean halo masses of the obscured and unobscured quasar populations. The obscured fraction of quasars for most of these

populations also fell below the observed obscured fraction range.

We similarly addressed the possible uncertainty in the $f_{\rm cov}-\log M_*$ relationships by varying the parameterizations to cover the parameter space between the Student's $t$-distribution-derived and Gaussian pdf-derived covering fraction curves, similar to what is shown in Figure 2 for the radiation-regulated unification model. We did this to account for the fact that the shape of the underlying $N_{\rm H}$ pdf is uncertain. We again find that there is nowhere in this parameter space that can simultaneously satisfy observational constraints on the dark matter halo masses for the obscured and unobscured quasars and the obscured fraction.

### 3.5. Implications for Evolution

In this work, we have explored various simple models that attempt to recover the clustering measurements of mid-IR-selected quasars by characterizing quasar obscuration as a function of either $\lambda_{\rm Edd}$ or host galaxy stellar mass. We found that these models could satisfy either dark matter halo mass measurements or the observed obscured fraction, but not both. This result strongly implies that evolution needs to be incorporated into quasar obscuration models to be able to understand the observed halo mass difference between obscured and unobscured populations of quasars.

One commonly invoked picture of quasar evolution is that quasar activity is triggered by a dramatic event such as a merger or disk instability. The quasar then remains active in an obscured state until it rids itself of obscuring material via radiative and mechanical feedback to become unobscured (e.g., Sanders et al. 1988; Di Matteo et al. 2005; Hopkins et al. 2008; Alexander & Hickox 2012; DiPompeo et al. 2017b; Hickox & Alexander 2018). Qualitatively, treating the effective obscuring covering fraction as a function of time in a quasar's evolution provides a simple explanation for the fact that obscured and unobscured quasars have different observed properties such as host dark matter halo mass. DiPompeo et al. (2017b) quantitatively showed that this evolutionary sequence is able to re-create clustering measurements. The key piece to evolutionary models is understanding the timescales at which the host galaxy and the quasar/black hole evolve. The model presented in DiPompeo et al. (2017b) assumed coevolution between the host galaxy and the black hole, but the black hole grew in spurts and its growth lagged behind that of the galaxy. The implication of this is that obscured quasars host black holes that are undermassive relative to what would be expected based on their host galaxy masses. This effect, coupled with a luminosity threshold, is enough to drive a difference in the average host dark matter halo mass between populations of obscured and unobscured quasars. Although it has been shown that the dusty torus does exist and that it can obscure a quasar along certain LOSs, any torus-obscuration model needs to consider a time dependence on the $M_*$–$M_{\rm BH}$ relationship to be able to properly re-create observations.

Separate from host galaxy or black hole properties, Powell et al. (2018) discussed the potential role of assembly bias and environment on the dark matter halo mass discrepancy between obscured and unobscured quasars. For a population of $z\sim 0.1$, X-ray-selected AGNs, the model presented in DiPompeo et al. (2017b) predicted a much smaller host halo mass difference than measured. Powell et al. (2018) argued that this implies that assembly bias, in which unobscured AGNs reside in more recently formed halos, could be driving a physical difference in AGN clustering. This is distinct from observed clustering differences arising as a selection effect due to the limiting luminosities of surveys. This interpretation also considers a time dependence on obscuration, albeit on a different timescale than that in DiPompeo et al. (2017b). Both assembly bias and event-driven evolution scenarios are viable to explain the observed clustering difference in mid-IR-selected quasars on their own or in conjunction with a torus/galaxy-scale obscuration model.

## 4. Summary and Conclusions

Observational studies of quasars have shown that obscured quasars preferentially reside in higher-mass dark matter halos, a result that contradicts the simplest models of unification by orientation (e.g., Hickox et al. 2011; DiPompeo et al. 2014, 2016a, 2017a; Donoso et al. 2014). Recent results presented for Compton-thin AGNs in Ricci et al. (2017) showed a strong relationship between the covering factor of an AGN's torus and its $\lambda_{\rm Edd}$. Using this empirical relationship, along with known $M_{\rm halo}$ and $\lambda_{\rm Edd}$ distributions, we constructed a simple model that sought to re-create the $M_{\rm halo}$ difference for obscured and unobscured quasars as seen in mid-IR quasar clustering measurements. We find that our model of radiation-regulated unification is not able to re-create clustering measurements while also producing samples of quasars that have an obscured fraction that falls within observations.

Using relationships between host galaxy gas content and stellar mass as presented in Buchner et al. (2017) and Pannella et al. (2009), it was also possible to model quasar obscuration as a function of its host galaxy's stellar mass. We find that although some of these models were able to produce host $M_{\rm halo}$ that fell within the range of clustering measurements, they are not viable since the obscured fractions for these populations were outside the observed range (e.g., Polletta et al. 2008; Treister et al. 2008; DiPompeo et al. 2016b; Yan et al. 2019). We also considered the effect of allowing our simulated quasars to be obscured by the parsec-scale dusty torus and by its host galaxy's interstellar gas. This model is able to produce a population of quasars that have an obscured fraction that falls within the observed range, but the dark matter halo mass difference between the obscured and unobscured populations is too small compared to what is calculated from mid-IR clustering measurements.

Some evolutionary paradigms of obscuration have been able to broadly recover observed dark matter halo masses of mid-IR-selected quasar populations (e.g., Di Matteo et al. 2005; Hopkins et al. 2008; DiPompeo et al. 2017b; Blecha et al. 2018). They assume coevolution between the larger-scale galaxy properties and the small-scale environment of the AGN via various physical processes such as mergers or feedback. It is worth noting that even though evolutionary models have been able to reproduce dark matter halo mass measurements, they have also struggled to recover obscured fractions that fall within the range of observations (e.g., DiPompeo et al. 2017b). Here we considered nonevolutionary physical models that describe how the properties of the galaxy or quasar could affect obscuring material on large and small scales. We implemented known empirical relationships between $M_{\rm halo}$, galaxy mass, and SMBH mass, as well as relationships between a quasar's covering fraction and its $\lambda_{\rm Edd}$ and between its host galaxy's stellar mass and $N_{\rm H}$ (Häring & Rix 2004; Pannella et al. 2009;

Moster et al. 2010; Tinker et al. 2010; Jones et al. 2016; Buchner et al. 2017; Ricci et al. 2017; Whitaker et al. 2017). We sought to determine whether these relationships, coupled with a luminosity threshold representative of the observational limitations of *WISE*, could recover the host $M_{\rm halo}$ calculated via clustering measurements, as well as an obscured fraction that fell within the range of observations. We found that these nonevolutionary approaches to modeling quasar evolution are not enough to be able to properly simulate observed populations of mid-IR-selected quasars. We could not simultaneously recover mean $M_{\rm halo}$ for our obscured and unobscured quasars and an obscured fraction that falls within the range of observations. The dusty torus and galaxy-scale dust and gas both likely play a role in quasar obscuration, but evolutionary models that invoke processes for AGN triggering and feedback such as event-driven radiative blowout still need to be considered to be able to model populations of observed mid-IR-selected quasars.

K.E.W. acknowledges support from the Dartmouth Fellowship. R.C.H. acknowledges support from the NSF through CAREER award 1554584 and from NASA through ADAP grant no. NNX16AN48G. G.T.R. acknowledges support from NASA-ADAP grant NNX17AF04G. A.D.M. acknowledges support from NSF grant AST-1616168. Thank you to the anonymous referee, whose input helped make this a stronger paper. We also thank Laurrane Lanz and Alberto Masini for their constructive input.

## ORCID iDs

Kelly E. Whalen https://orcid.org/0000-0002-8571-9801
Ryan C. Hickox https://orcid.org/0000-0003-1468-9526
Michael A. DiPompeo https://orcid.org/0000-0001-6788-1701
Gordon T. Richards https://orcid.org/0000-0002-1061-1804

## References

Alexander, D. M., Brandt, W. N., Smail, I., et al. 2008, AJ, 135, 1968
Alexander, D. M., & Hickox, R. C. 2012, NewAR, 56, 93
Antonucci, R. 1993, ARA&A, 31, 473
Antonucci, R. R. J., & Miller, J. S. 1985, ApJ, 297, 621
Assef, R. J., Stern, D., Kochanek, C. S., et al. 2013, ApJ, 772, 26
Baldwin, J. A. 1977, ApJ, 214, 679
Barthelmy, S. D., Barbier, L. M., Cummings, J. R., et al. 2005, SSRv, 120, 143
Baumgartner, W. H., Tueller, J., Markwardt, C. B., et al. 2013, ApJS, 207, 19
Behroozi, P. S., Conroy, C., & Wechsler, R. H. 2010, ApJ, 717, 379
Blecha, L., Snyder, G. F., Satyapal, S., & Ellison, S. L. 2018, MNRAS, 478, 3056
Buchner, J., & Bauer, F. E. 2017, MNRAS, 465, 4348
Buchner, J., Schulze, S., & Bauer, F. E. 2017, MNRAS, 464, 4545
Burtscher, L., Davies, R. I., Graciá-Carpio, J., et al. 2016, A&A, 586, A28
Chen, C.-T. J., Hickox, R. C., Alberts, S., et al. 2015, ApJ, 802, 50
Coil, A. L., Hennawi, J. F., Newman, J. A., Cooper, M. C., & Davis, M. 2007, ApJ, 654, 115
Conroy, C., & White, M. 2013, ApJ, 762, 70
Croom, S. M., Boyle, B. J., Shanks, T., et al. 2005, MNRAS, 356, 415
Croom, S. M., Smith, R. J., Boyle, B. J., et al. 2004, MNRAS, 349, 1397
da Ângela, J., Shanks, T., Croom, S. M., et al. 2008, MNRAS, 383, 565
Di Matteo, T., Springel, V., & Hernquist, L. 2005, Natur, 433, 604
DiPompeo, M. A., Hickox, R. C., Eftekharzadeh, S., & Myers, A. D. 2017a, MNRAS, 469, 4630
DiPompeo, M. A., Hickox, R. C., & Myers, A. D. 2016a, MNRAS, 456, 924
DiPompeo, M. A., Hickox, R. C., Myers, A. D., & Geach, J. E. 2017b, MNRAS, 464, 3526
DiPompeo, M. A., Myers, A. D., Hickox, R. C., Geach, J. E., & Hainline, K. N. 2014, MNRAS, 442, 3443
DiPompeo, M. A., Runnoe, J. C., Hickox, R. C., Myers, A. D., & Geach, J. E. 2016b, MNRAS, 460, 175
Donoso, E., Yan, L., Stern, D., & Assef, R. J. 2014, ApJ, 789, 44
Draine, B. T. 2003, ARA&A, 41, 241
Eftekharzadeh, S., Myers, A. D., White, M., et al. 2015, MNRAS, 453, 2779
Fan, X. 2006, NewAR, 50, 665
Fitzpatrick, E. L. 1999, PASP, 111, 63
Frank, J., King, A., & Raine, D. J. 2002, Accretion Power in Astrophysics, 3rd ed. (Cambridge: Cambridge Univ. Press), 398
Gehrels, N., Chincarini, G., Giommi, P., et al. 2004, ApJ, 611, 1005
Goulding, A. D., Alexander, D. M., Bauer, F. E., et al. 2012, ApJ, 755, 5
Guo, Q., White, S., Li, C., & Boylan-Kolchin, M. 2010, MNRAS, 404, 1111
Hainline, K. N., Hickox, R. C., Carroll, C. M., et al. 2014, ApJ, 795, 124
Häring, N., & Rix, H.-W. 2004, ApJL, 604, L89
Hickox, R. C., & Alexander, D. M. 2018, ARA&A, 56, 625
Hickox, R. C., Jones, C., Forman, W. R., et al. 2007, ApJ, 671, 1365
Hickox, R. C., Jones, C., Forman, W. R., et al. 2009, ApJ, 696, 891
Hickox, R. C., Myers, A. D., Brodwin, M., et al. 2011, ApJ, 731, 117
Hickox, R. C., Myers, A. D., Greene, J. E., et al. 2017, ApJ, 849, 53
Hopkins, P. F., Hernquist, L., Cox, T. J., & Kereš, D. 2008, ApJS, 175, 356
Hopkins, P. F., Somerville, R. S., Hernquist, L., et al. 2006, ApJ, 652, 864
Jones, M. L., Hickox, R. C., Black, C. S., et al. 2016, ApJ, 826, 12
Jones, M. L., Hickox, R. C., Mutch, S. J., et al. 2019, ApJ, 881, 110
Kelly, B. C., & Merloni, A. 2012, AdAst, 2012, 970858
King, A. R. 2010, MNRAS, 408, L95
Klindt, L., Alexander, D. M., Rosario, D. J., Lusso, E., & Fotopoulou, S. 2019, MNRAS, 488, 3109
Komatsu, E., Smith, K. M., Dunkley, J., et al. 2011, ApJS, 192, 18
Kormendy, J., & Ho, L. C. 2013, ARA&A, 51, 511
Krimm, H. A., Holland, S. T., Corbet, R. H. D., et al. 2013, ApJS, 209, 14
Krumpe, M., Miyaji, T., Coil, A. L., & Aceves, H. 2012, ApJ, 746, 1
Lamastra, A., Menci, N., Maiolino, R., Fiore, F., & Merloni, A. 2010, MNRAS, 405, 29
Leighly, K. M. 2004, ApJ, 611, 125
Lewis, A., Challinor, A., & Lasenby, A. 2000, ApJ, 538, 473
Luo, B., Brandt, W. N., Hall, P. B., et al. 2015, ApJ, 805, 122
Lusso, E., & Risaliti, G. 2016, ApJ, 819, 154
Merloni, A., Bongiorno, A., Brusa, M., et al. 2014, MNRAS, 437, 3550
Moster, B. P., Somerville, R. S., Maulbetsch, C., et al. 2010, ApJ, 710, 903
Myers, A. D., Brunner, R. J., Nichol, R. C., et al. 2007, ApJ, 658, 85
Netzer, H. 2015, ARA&A, 53, 365
Netzer, H., & Trakhtenbrot, B. 2014, MNRAS, 438, 672
Padovani, P., Alexander, D. M., Assef, R. J., et al. 2017, A&ARv, 25, 2
Pannella, M., Carilli, C. L., Daddi, E., et al. 2009, ApJL, 698, L116
Pérez-González, P. G., Rieke, G. H., Villar, V., et al. 2008, ApJ, 675, 234
Polletta, M., Weedman, D., Hönig, S., et al. 2008, ApJ, 675, 960
Powell, M. C., Cappelluti, N., Urry, C. M., et al. 2018, ApJ, 858, 110
Predehl, P., & Schmitt, J. H. M. M. 1995, A&A, 500, 459
Ramos Almeida, C., & Ricci, C. 2017, NatAs, 1, 679
Ricci, C., Trakhtenbrot, B., Koss, M. J., et al. 2017, Natur, 549, 488
Richards, G. T., Strauss, M. A., Fan, X., et al. 2006, AJ, 131, 2766
Ross, N. P., Shen, Y., Strauss, M. A., et al. 2009, ApJ, 697, 1634
Sanders, D. B., Soifer, B. T., Elias, J. H., et al. 1988, ApJ, 325, 74
Schnorr-Müller, A., Davies, R. I., Korista, K. T., et al. 2016, MNRAS, 462, 3570
Shankar, F., Weinberg, D. H., & Miralda-Escudé, J. 2009, ApJ, 690, 20
Shen, Y., Strauss, M. A., Oguri, M., et al. 2007, AJ, 133, 2222
Shen, Y., Strauss, M. A., Ross, N. P., et al. 2009, ApJ, 697, 1656
Silk, J., & Rees, M. J. 1998, A&A, 331, L1
Springel, V., Di Matteo, T., & Hernquist, L. 2005, MNRAS, 361, 776
Tinker, J. L., Robertson, B. E., Kravtsov, A. V., et al. 2010, ApJ, 724, 878
Treister, E., Krolik, J. H., & Dullemond, C. 2008, ApJ, 679, 140
Treister, E., Schawinski, K., Urry, C. M., & Simmons, B. D. 2012, ApJL, 758, L39
Urry, C. M., & Padovani, P. 1995, PASP, 107, 803
Usman, S. M., Murray, S. S., Hickox, R. C., & Brodwin, M. 2014, ApJL, 788, L3
Veale, M., White, M., & Conroy, C. 2014, MNRAS, 445, 1144
Werner, M. W., Roellig, T. L., Low, F. J., et al. 2004, ApJS, 154, 1
Whitaker, K. E., Pope, A., Cybulski, R., et al. 2017, ApJ, 850, 208
Woo, J.-H., Treu, T., Malkan, M. A., & Blandford, R. D. 2008, ApJ, 681, 925
Wright, E. L., Eisenhardt, P. R. M., Mainzer, A. K., et al. 2010, AJ, 140, 1868
Yan, W., Hickox, R. C., Hainline, K. N., et al. 2019, ApJ, 870, 33
Zou, F., Yang, G., Brandt, W. N., & Xue, Y. 2019, ApJ, 878, 11